Research Square

Preprints are preliminary reports that have not undergone peer review.
They should not be considered conclusive, used to inform clinical practice,
or referenced by the media as validated information.

Impact of Wall Roughness on the spontaneous ignition of pressurized hydrogen released into a tube

Gang Luo

luogang36150163.com

Nanjing Tech University

Lijing Zhang

Nanjing Tech University

Research Article

Keywords: Pressurized Hydrogen, Spontaneous Ignition, Wall roughness, Large Eddy Simulation (LES)

Posted Date: November 9th, 2026

DOI: https://doi.org/10.21203/rs.3.rs-11370052/v1

License: This work is licensed under a Creative Commons Attribution 4.0 International License.
Read Full License

Additional Declarations: No competing interests reported.

Impact of Wall Roughness on the spontaneous ignition of pressurized hydrogen released into a tube

Gang Luo[ab], Lijing Zhang[a1]

a College of Safety Science and Engineering, Nanjing Tech University, Nanjing 211816, China

b Zhejiang College of Security Technology, Department of emergency and technology, Wenzhou 325016, China.

Abstract:

While significant advancements have been made in understanding the spontaneous ignition of pressurized hydrogen during accidental releases, the aerodynamic effects of tube surface conditions remain critically underexplored. This paper presents a numerical investigation into the effects of equivalent sand-grain wall roughness (Ra) on the ignition mechanisms, shock wave propagation, and non-premixed flame evolution of pressurized hydrogen releases. Utilizing Large Eddy Simulation (LES) coupled with a mixture averaged transport model and an Improved Partially Stirred Reactor (PaSR) combustion model, the study evaluates the transient dynamics across absolutely smooth (Ra = 0 mm) and varying rough (Ra = 0.1, 0.5, 1.0 mm) tube boundary conditions. The analysis demonstrates that wall roughness significantly suppresses the radial expansion and central coalescence of the flame front, ultimately leading to the dissipation of the central reaction zone at high roughness scales. Conversely, roughness-induced localized vortices drastically intensify boundary layer combustion. Furthermore, wall roughness introduces a non-linear suppression of leading shock wave velocities and elevates the critical burst pressure threshold required for spontaneous ignition from 3.2 MPa to 3.5 MPa , driven by intense near-wall momentum and thermal dissipation. The findings provide critical theoretical foundations for the quantitative risk assessment of hydrogen infrastructure and inform future iterations of tube safety standards.

Keywords: Pressurized Hydrogen, Spontaneous Ignition,Wall roughness, Large Eddy Simulation (LES)

1. Introduction

In the rapid deployment of pressurized hydrogen tube networks and refueling infrastructure, ensuring operational safety against accidental releases is of paramount importance. In pressurized hydrogen infrastructure, practical tube inner

[1] Corresponding authors at: College of Safety Science and Engineering, Nanjing Tech University, Nanjing 211816, China.
E-mail addresses:zhanglj@njtech.edu.cn

walls invariably exhibit microscopic surface roughness due to manufacturing tolerances, mechanical wear, chemical corrosion, or particulate deposition. As an essential aerodynamic disturbance source, wall roughness (R_a) strongly modulates boundary layer transition, amplifying local shear stresses and turbulent fluctuations. Spontaneous ignition following pressurized hydrogen releases is primarily governed by shock-induced transient aerodynamic heating of the near-wall medium and subsequent ignition of the hydrogen-air mixture within the boundary layer. Consequently, wall roughness inherently alters shock reflection/propagation dynamics, ignition delay, flame morphology, and subsequent combustion propagation. Incorporating wall roughness into the mechanistic framework of pressurized hydrogen ignition not only enriches fundamental release-ignition theory, but also provides critical engineering insight for safety design and quantitative risk assessment in hydrogen transport systems.

The impact of wall roughness on internal flow topologies and transport phenomena is well-documented. Roughness elements destabilize the near-wall viscous sublayer, precipitating premature laminar-to-turbulent transition and intensifying near-wall momentum exchange(Wang et al., 2026) . In confined gaseous explosions, roughness is widely recognized to facilitate flame acceleration (FA) and promote deflagration-to-detonation transition (DDT)(Maeda et al., 2019; Zhao et al., 2024) . For instance, Li et al. (Li et al., 2026) demonstrated through premixed CH_4/air detonation tests that roughness arrays promote DDT via localized shock reflections and turbulence-chemistry interactions. Wang et al.(Wang et al., 2026) experimentally verified that wall roughness significantly accelerates flame propagation in hydrogen-oxygen blends at H_2 fractions below 40%. Furthermore, roughness geometry exerts nonlinear effects on flame acceleration, shock passage over micro-cavities induces intense vortex shearing and viscous dissipation, fostering local “hot spots” that spawn micro-detonations(G. Yu. Bivol et al., 2024). Nevertheless, some roughness heights(Yan et al., 2023) or prolonged rough surface spans (G.Yu. Bivol et al., 2024) have been shown to attenuate detonation front propagation. Zhang et al.(Zhang et al., 2026) also revealed through numerical modeling that elevated roughness can suppress near-wall non-premixed combustion by isolating fuel-oxidizer interfacial mixing.

Although existing literature extensively addresses roughness effects on premixed flame dynamics, FA, and detonation development, the coupled role of wall roughness in pressurized hydrogen ignition and subsequent non-premixed flame evolution remains largely unaddressed. To address these deficiencies, this paper focuses on three principal objectives: (1) formulating a calibrated equivalent sand-grain roughness boundary within high-resolution grids to quantify roughness effects on shock wave intensity and velocity field evolution; (2) characterizing the dynamics of roughness-induced boundary layer vortex structures and their regulatory role in

transient fuel-air mixing; and (3) systematically elucidating the mechanisms by which roughness height governs ignition delays, thermo-fluid dynamic fields, and flame propagation regimes.

2. Theoretical Framework and Computational Setup

2.1 Numerical models

To accurately capture the transient compressibility, shock-boundary layer interactions, and turbulent reactive scalars characterizing pressurized hydrogen spontaneous ignition, the present study utilizes the Large Eddy Simulation (LES) framework. To achieve sub-grid stress closure, this study employs the one-equation dynamicKEqn sub-grid turbulent kinetic energy model. This approach is motivated by a systematic re-evaluation of which terms within the model can be dynamically determined. The transport equation is expressed as follows(Kajishima and Nomachi, 2006):

$$\frac{\partial(\rho\overline{u_i})}{\partial t} + \overline{u_j}\frac{\partial(\rho\overline{u_i})}{\partial x_j} = -\frac{\partial(\bar{p} + \frac{2}{3}K_{SGS})}{\partial x_i} + \frac{\partial\overline{\tau_{ij}}}{\partial x_j} \tag{1}$$

The viscous stress tensor $\overline{\tau_{ij}}$ is computed as:

$$\overline{\tau_{ij}} = 2\ (\nu_{SGS} + \nu)\ \overline{S_{ij}} \tag{2}$$

The viscosity coefficient, ν, is calculated employing the method from the LaminarReactingFoam solver, as detailed in a previous article concerning its influence on pressurized hydrogen ignition(Luo et al., 2025). In addition, the SGS eddy viscosity ν_{SGS} is defined by Equation (3):

$$\nu_{SGS} = C_\nu \Delta_\nu \sqrt{K_{SGS}} \tag{3}$$

Here, K_{SGS} denotes the SGS kinetic energy. Given that the coefficient $C_\nu$remains non-negative, which promotes numerical stability in computing Equation (9). The transport equation for K_{SGS}, presented as Equation (1), is solved to obtain its value(Huang and Li, 2010; Kajishima and Nomachi, 2006; Kim, n.d.):

$$\frac{\partial(K_{SGS})}{\partial t} + \overline{u_j}\frac{\partial(K_{SGS})}{\partial x_j} = -\tau_{ij}\overline{S_{ij}} - C_\varepsilon\frac{K_{SGS}^{3/2}}{\bar{\Delta}} + \frac{\partial}{\partial x_j}[(C_d\Delta_\nu\sqrt{K_{SGS}} + \nu)\frac{\partial K_{SGS}}{\partial x_j}] \tag{4}$$

The calculation of model constants, such as C_ε and C_d, has been derived and

demonstrated in detail in the literature(Kim, n.d.) and will not be reiterated here. It is noteworthy that compared to the traditional dynamic Smagorinsky model, the dynamicKEqn model resolves the convergence issues caused by negative coefficients and has found extensive numerical application in channel flow simulations(Liu and Lu, 2005; Qi et al., 2022; Ranjan et al., 2020).

For the turbulence-chemistry interaction, an Improved Partially Stirred Reactor (Improved PaSR) combustion model is developed. The filtered reaction rate $\overline{\dot{\omega}_\imath}$ is calculated by summing the contributions of all reactions(Ingenito and Bruno, 2010):

$$\overline{\dot{\omega}_\imath} = \sum_{\mathrm{j}=1}^{\mathrm{n}} \gamma_\mathrm{j}^* \, \overline{\dot{\omega}_{\imath,\mathrm{J}}} \tag{5}$$

For each reaction j, $\gamma_\mathrm{j}^* = \tau_{\mathrm{ch,j}}/(\tau_{\mathrm{ch,j}} + \tau_\mathrm{m})$. Chemical time scale, $\tau_{\mathrm{ch,j}}$, is determined by the shortest residence time among all reactants involved in that reaction:

$$\tau_{ch,j} = \min_{i \in reactants} \left| \frac{\rho Y_i}{\dot{\omega}_{i,j}} \right| \tag{6}$$

The mixing time scale τ_m is defined as the geometric mean of the Kolmogorov time scale τ_k and the time scale of sub-grid velocity stretch τ_Δ:

$$\tau_m = \sqrt{\tau_k \tau_\Delta} \tag{7}$$

Validations in scramjet combustors demonstrated a 25% improvement in wall pressure predictions compared to the PaSR combustion model(Xiang et al., 2020).

The chemical kinetics are governed by a well-validated 9-species, 19-step hydrogen/air skeletal reaction mechanism(Burke et al., 2012), coupled with a mixture-averaged transport formulation. The accurate modeling of intermediate species diffusion is particularly critical for hydrogen, as its low Lewis number renders it highly susceptible to thermo-diffusive instabilities, resulting in localized enrichment of the flame front and superadiabatic temperature zones.

2.2 Problem description

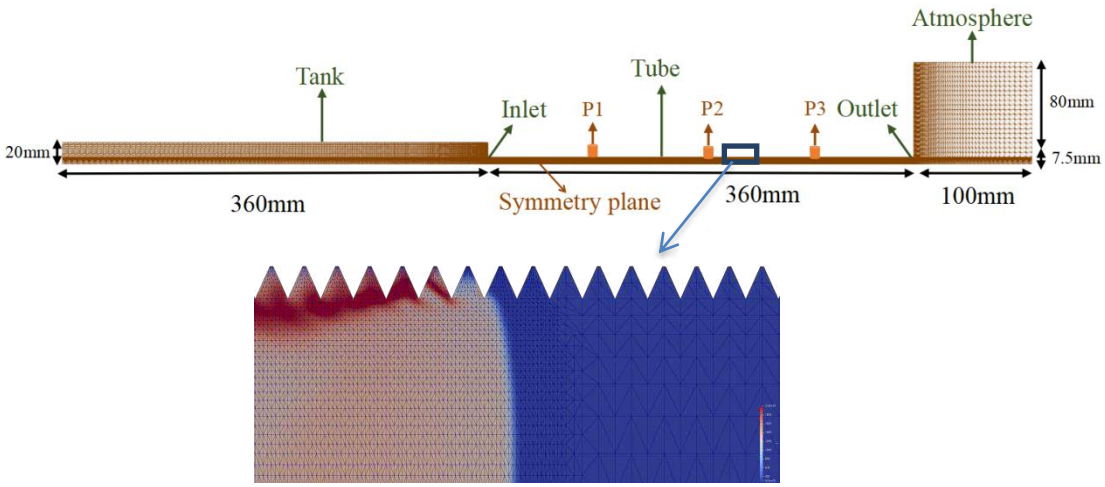


Fig.1 The physical model and computational domain

As shown in Figure1, a 2D symmetric simulation is performed in the paper. The computational domain includes a high-pressure storage tank, a tube, and the external atmosphere. A cylindrical tube, measuring 40 mm in diameter and 360 mm in length, functions as the high-pressure storage tank. An attached downstream tube has dimensions of 360 mm in length and 15 mm in height. The dimensions of the external atmosphere are 100 mm in length and 175 mm in height. To decrease the computation cost, the symmetryPlane boundary condition is used in the construction of the computational domain. Pressure monitors P1, P2, and P3 are set up at 90 mm, 180 mm, and 270 mm, respectively from the burst disk.

In practical industrial infrastructure, wall roughness is typically specified as R_a=0.2mm for mildly corrosive gases (e.g., hydrocarbons and air), R_a=0.5mm for standard liquids like water, and up to R_a=1.0 mm for highly corrosive fluids such as acids and alkalis. To ensure the broad applicability of the computational results, three discrete wall roughness cases were investigated: Ra = 0.1 mm, 0.5 mm, and 1.0 mm. To facilitate robust grid generation, the individual roughness elements were geometrically simplified into triangular micro-structures.

Regarding the computational meshing strategy, a baseline background grid resolution of approximately 250μm was adopted to balance computational overhead with the spatial requirements of the minimum roughness height (Ra = 0.1 mm). To rigorously resolve the severe aerodynamic heating and viscous shear stresses within the boundary layer, the first layer of the wall-adjacent mesh was locally refined to 50μm, which allocates two grid cells across the height of the smallest roughness element. Furthermore, the implementation of Adaptive Mesh Refinement (AMR) dynamically scales the local grid resolution, ultimately yielding eight cells across the minimum roughness unit. The refinement criterion is based on the magnitude of the density gradient ($|\nabla\rho|$), with a trigger threshold of 200. A maximum of three refinement levels is permitted every 10 time steps, utilizing 20 buffer layers to

maintain numerical stability and gradient smoothness.

Boundary conditions are listed in Table 1. The initial fields for pressure(P) and the mole fractions of H_2, O_2 and N_2 are set as:

$$(P, H_2, O_2, N_2) = \begin{pmatrix} (5.89\text{MPa}, 1,0,0) & x <= 0.001 + 0.001 * \cos(2\pi y/0.015) \\ (0.101325\text{MPa}, 0,0.21,0.79) & x > 0.001 + 0.001 * \cos(2\pi y/0.015) \end{pmatrix} \quad (8)$$

Table 1 Boundary conditions

	Tank and tube		Atmosphere	
	boundarywall	symmetryPlane	boundarywall	symmetryPlane
P(kg/m/s^2)	zeroGradient	symmetry	waveTransmissive	symmetry
T(K)	zeroGradient	symmetry	inletOutlet	symmetry
U(m/s)	noSlip	symmetry	inletOutlet	symmetry
H2(-)	zeroGradient	symmetry	inletOutlet	symmetry
N2(-)	zeroGradient	symmetry	inletOutlet	symmetry
O2(-)	zeroGradient	symmetry	inletOutlet	symmetry
Yi(-)	zeroGradient	symmetry	inletOutlet	symmetry

2.3 Assessment of LES Fidelity

The reliability and physical fidelity of Large Eddy Simulations are fundamentally dependent on the proportion of turbulent kinetic energy that is directly resolved by the grid versus the proportion that is modeled by the SGS closure. According to the widely accepted Pope criterion, a high-quality LES should directly resolve at least 80% of the total turbulent kinetic energy, ensuring that the filter cut-off lies well within the inertial subrange of the turbulent energy cascade.

The resolved turbulent kinetic energy fraction, η, is calculated using the following formulation:

$$\eta = \frac{K_{RES}}{K_{SGS}} = 1 - \frac{K_{SGS}}{K_{TOT}} \quad (9)$$

Where K_{TOT} is the total turbulent kinetic energy, representing the sum of the resolved turbulent kinetic energy (K_{RES}) and the sub-grid scale turbulent kinetic energy (K_{SGS}). The resolved portion is computed directly from the resolved velocity fluctuations (u', v' and w') in the three spatial directions:

$$K_{RES} = 1/2(u'^2 + v'^2 + w'^2) \quad (10)$$

Within the dynamicKEqn framework utilized in this study, the sub-grid turbulent kinetic energy K_{SGS} is distinctively calculated leveraging the sub-grid kinematic eddy viscosity (ν_{SGS}) and the local filter width (Δ), scaled by the dynamic Smagorinsky coefficient (C_s):

$$K_{SGS} = \frac{v_{SGS}^2}{(C_S\Delta)^2} \tag{11}$$

As shown in Figure 2, spatial evaluations of η were conducted at 150 μs after rupture across three varying base grid resolutions: 0.5mm, 0.25 mm, and 0.1 mm.

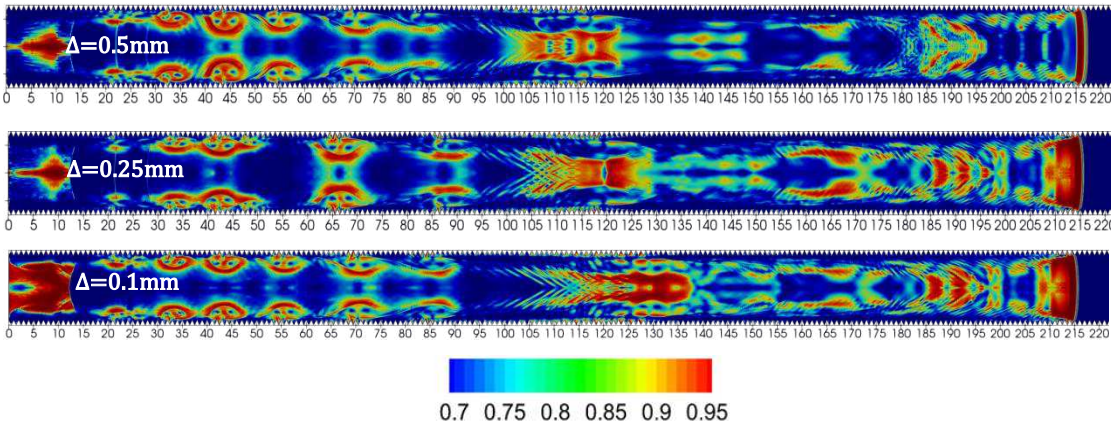


Fig.2 Spatial evolution of the percentage of the resolved turbulent kinetic energy

The spatial distribution demonstrated that across all three grids, the vast majority of the turbulent domain successfully resolved over 80% of the kinetic energy. Predictably, resolution quality improved with finer meshes. Specifically, within the highly turbulent zones, such as the highly corrugated flame front and the preheated region trailing the precursor shock, both the 0.25 mm and 0.1 mm grids achieved resolution rates significantly exceeding the 80% threshold, approaching 95% in critical reaction zones. Balancing computational efficiency, numerical stability, and the strict requirement for high-fidelity physics capture, the 0.25mm base grid, augmented by the aggressive AMR strategy, was deemed optimal and fully sufficient for the current investigation.

3.Results and discussion

3.1 Effect of Wall Roughness on Transient Flame Morphology

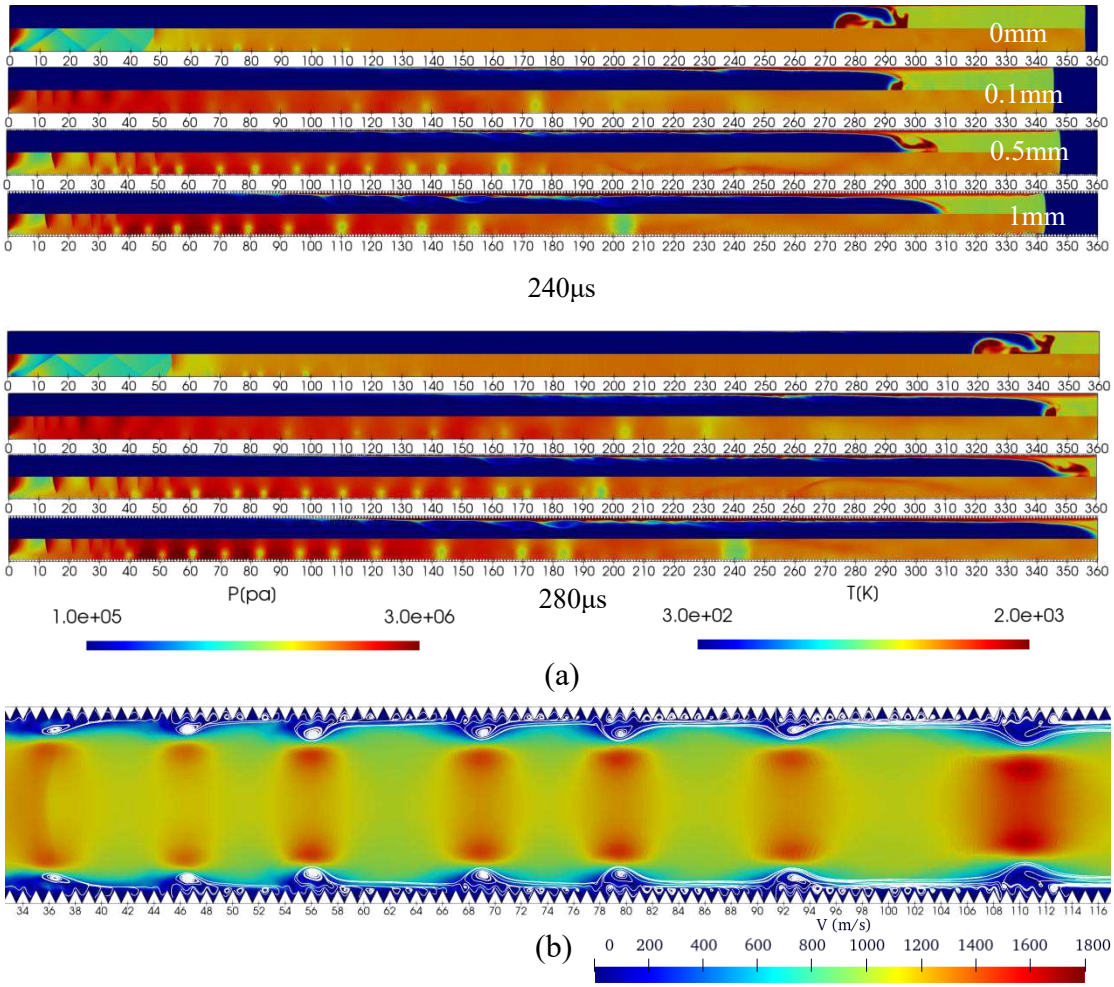


Fig. 3 At 5.89 MPa burst pressure: (a) pressure (top) and temperature (bottom) contours inside the pipe for four different wall roughnesses, and (b) velocity streamlines at Ra = 1 mm

Figure 3(a) presents the temporal evolution of the flame morphology (top) and pressure contours (bottom) from 0 μs to 280 μs following a burst pressure of 5.89 MPa, comparing four distinct wall roughness conditions (0, 0.1, 0.5, and 1 mm, respectively).

During the initial phase of flame development (10 μs to 50 μs), shock-induced compression universally triggers ignition within the boundary layer across all wall configurations. The criteria for spontaneous ignition as suggested by Rudy et al.(Rudy et al., 2014) are implemented: ignition occurs when the temperature exceeds 1500 K. Following this localized early ignition, the flame front propagates downstream. The interaction and reflection of the shock wave against the non-uniform hydrogen-air interface and the high density gradient boudary layer induce baroclinic torques. This triggers the Richtmyer-Meshkov (R-M) instability, which precipitates mild wrinkling of the initial flame front. While the evolutionary trends remain largely consistent across all cases during this stage, the viscous drag exerted

by the roughness elements on the near-wall fluid becomes discernible, progressively inducing a gradual stretching within the boundary layer of the roughened pipes.

Progressing into the mid-to-late stages (100 μs to 280 μs), wall roughness governs a profound morphological divergence in the flame structure, particularly concerning boundary layer expansion and inward radial convergence. Elevated surface roughness dramatically attenuates the flame's ability to merge and expand toward the pipe core. For the perfectly smooth wall (0 mm), the central flame front merges and expands to form pronounced single and double mushroom-like structures. In contrast, as the roughness (Ra) increases towards 1 mm, the radial growth of the flame into the core is severely impeded, preventing the formation of any mushroom-like topologies. Notably, in the extreme Ra = 1 mm case, the central flame undergoes distinct local extinction and dissipation during the final stages (240 μs and 280 μs).

Conversely, near-wall combustion intensifies proportionally with increasing roughness, resulting in a substantially broadened reaction zone. Both the flame thickness and axial length within the boundary layer increase visibly as the roughness height scales up. As depicted in Figure 3(b), the localized velocity contours and flow streamlines extracted at 240 μs for the Ra = 1 mm case demonstrate that roughness elements introduce severe aerodynamic perturbations. The profound velocity gradient between the high-speed mainstream core and the decelerated near-wall flow triggers the Kelvin-Helmholtz (K-H) instability. This shear driven mechanism spawns dense vortex clusters within and immediately downstream of the roughness cavities. These roughness-induced vortices drastically augment the turbulent mixing between the unburned mixture and hot combustion products, thereby accelerating localized chemical kinetics. Thermodynamically, this intense near-wall heat release and viscous vortex dissipation heavily deplete the transverse momentum and energy required for core-ward expansion, ultimately dictating the stagnation and dissipation of the central flame.

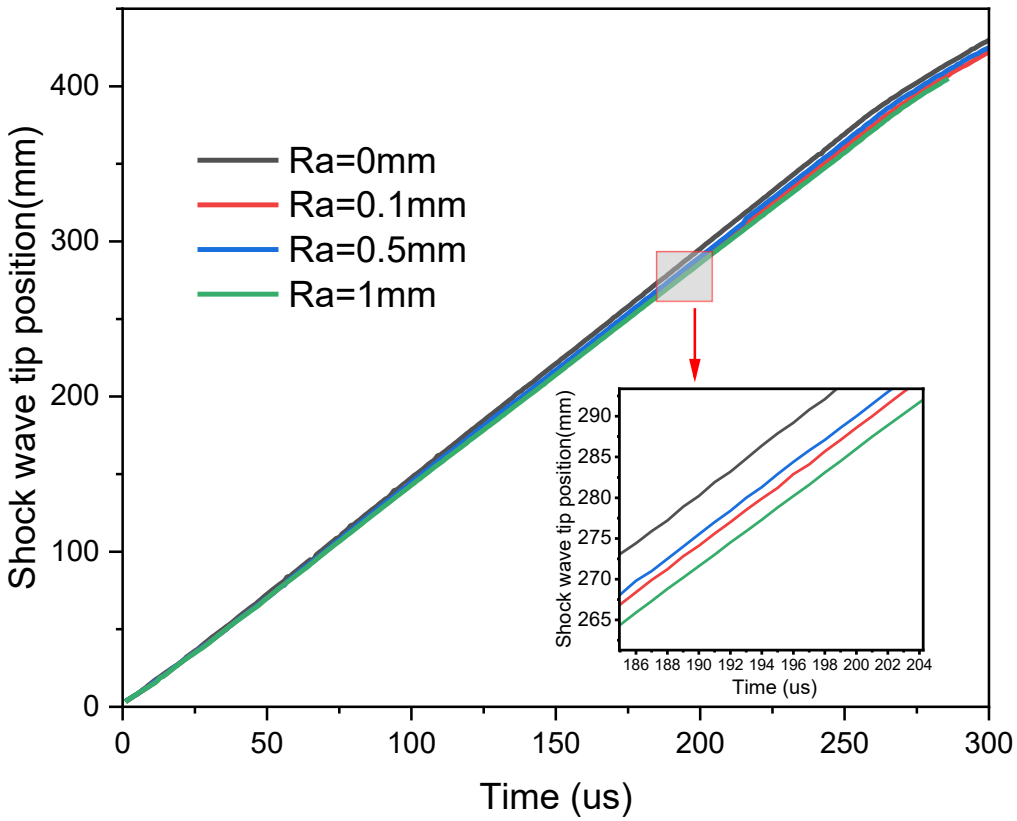


Fig. 4 Time history of the shock front location

To quantify the global dynamic influence of roughness, Figure 4 presents the time history of the shock front location. Globally, surface roughness consistently attenuates the shock propagation velocity, yielding shallower propagation slopes relative to the smooth wall. Interestingly, this attenuation manifests highly nonlinear characteristics. As highlighted in the magnified inset, the 0.1 mm roughness suppresses the shock more effectively than the 0.5 mm case, while the 1 mm condition imposes the maximum deceleration. Such non-monotonic behavior corroborates prior experimental observations of roughness effects on premixed in-pipe detonations(Zhong and Gou, 2021), underscoring the complex, scale-dependent modulation of flame dynamics by near-wall vortex structures. While existing literature primarily links higher roughness to accelerated premixed deflagration-to-detonation transitions (DDT), experimental data remains scarce for transient ignition and forward propagating boundary flames following pressurized hydrogen releases. From a numerical perspective, this study establishes that while wall roughness accelerates boundary layer combustion, it simultaneously prevents transverse flame propagation into the unburned core.

3.2Effect of Wall Roughness on Flow Field Parameters

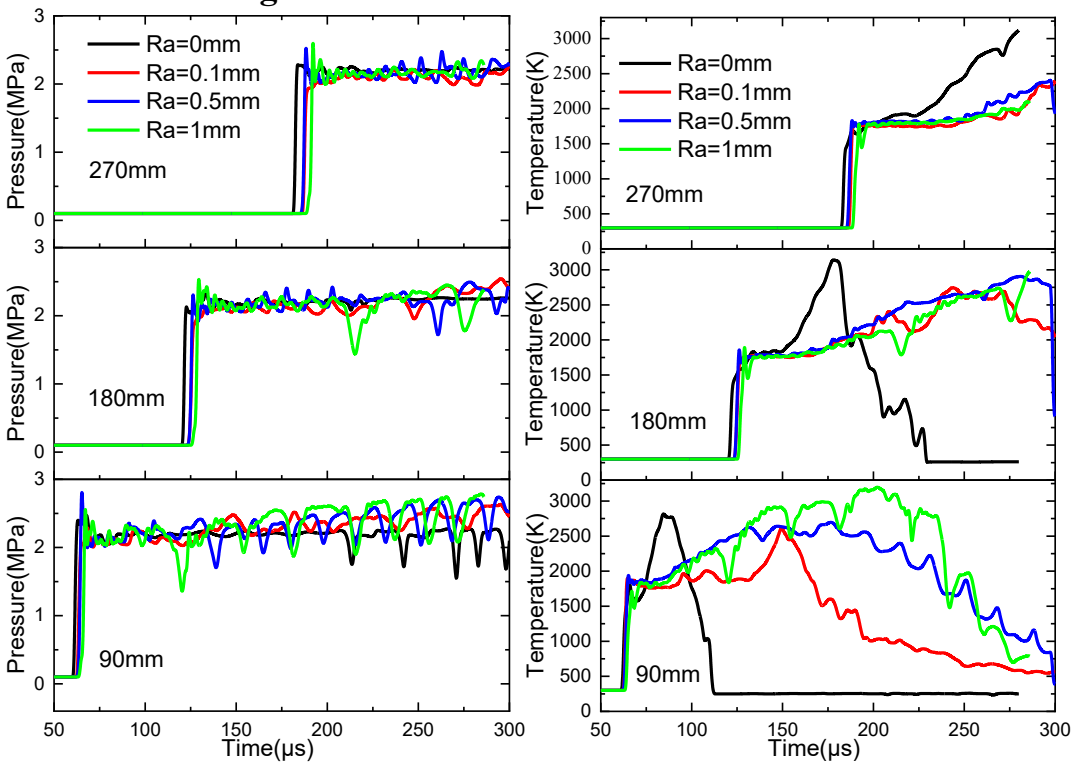


Fig. 5 Time histories of pressure and flame temperature at three monitoring points

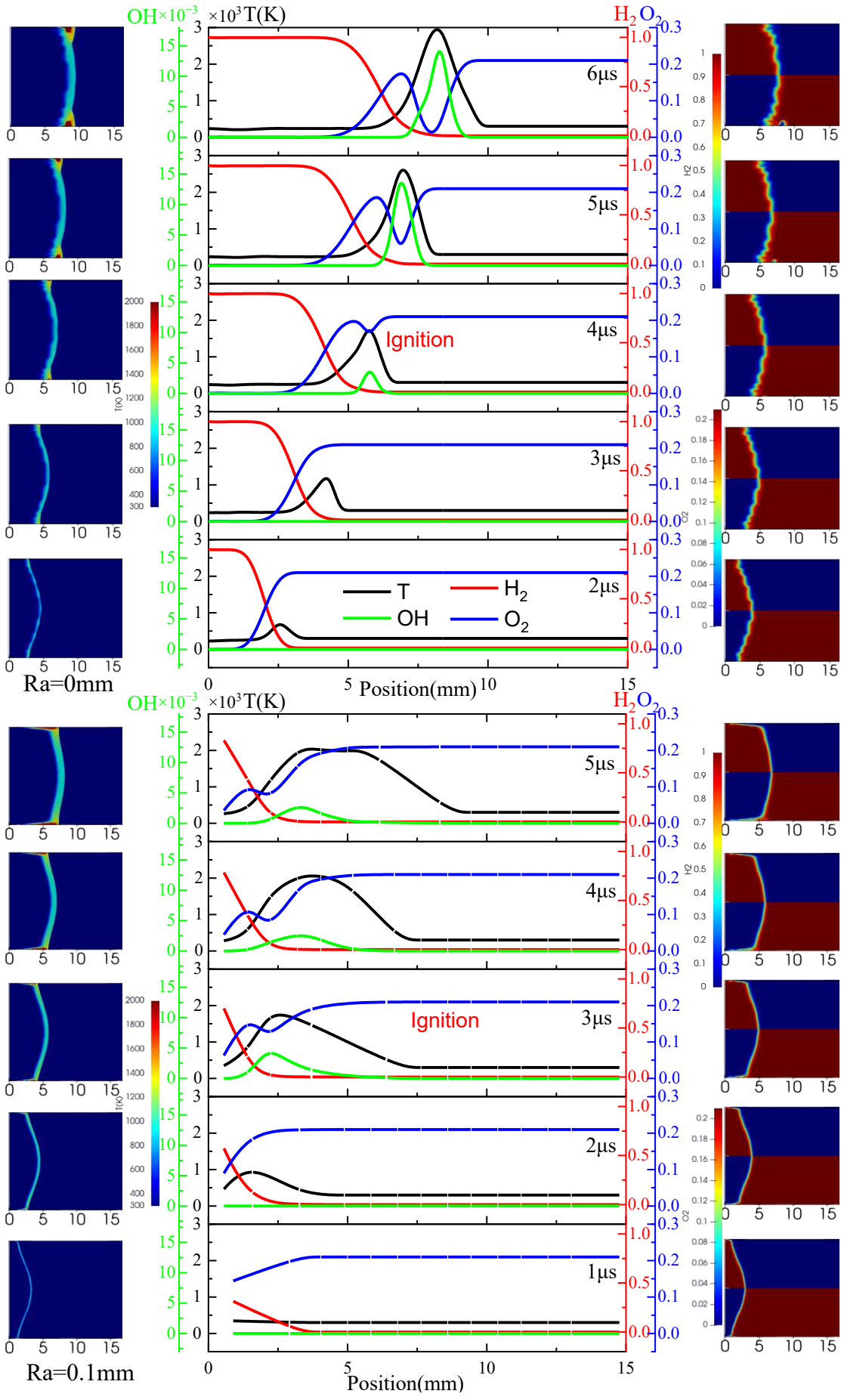
Figures 5(a) and (b) present the time histories of pressure and flame temperature at three monitoring points (90 mm, 180 mm, and 270 mm) inside the tube under a 5.89 MPa burst pressure for various wall roughnesses (Ra = 0, 0.1, 0.5, and 1 mm). Over the evolution period from 0 μs to 300 μs, both sets of curves thoroughly record the transient dynamics of the shock wave arrival, flame front passage, and subsequent combustion states.

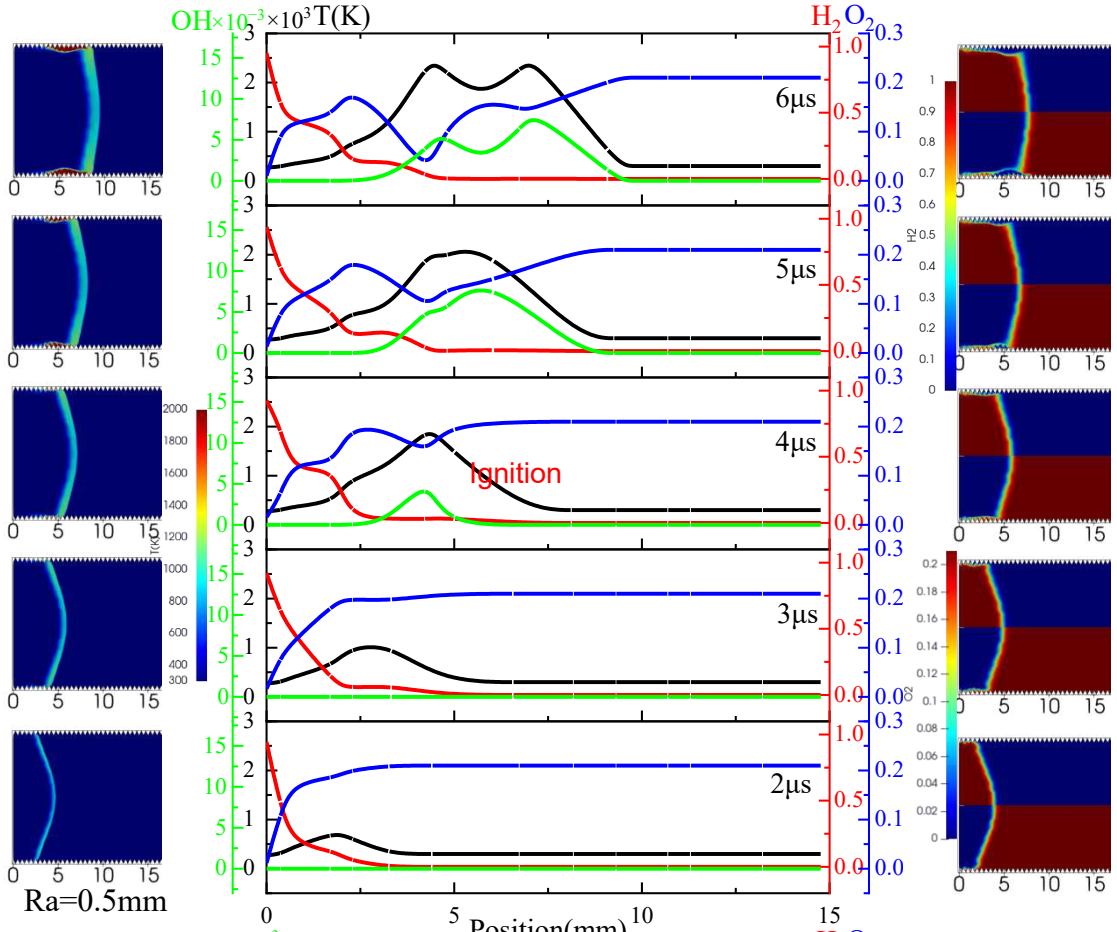
Regarding the pressure field evolution, the arrival time of the shock wave at each monitoring point and the morphology of the induced pressure jump are significantly affected by wall roughness. As wall roughness increases, the arrival time of the leading shock wave at the 90 mm, 180 mm, and 270 mm locations exhibits a systematic delay (an overall rightward shift of the curves), which is consistent with the shock positions depicted in Fig. 4. Concurrently, the peak pressure demonstrates a spatially non-monotonic evolution, at the upstream section of the pipe (90 mm), the shock-induced transient peak pressure inversely strengthens with increasing roughness (i.e., 1 mm > 0.5 mm > 0.1 mm). However, as the flow propagates toward the mid-to-downstream sections (180 mm and 270 mm), the mean pressure level for the 1 mm roughness case gradually attenuates, eventually

reversing to become slightly lower than those of the 0.5 mm and 0.1 mm cases.

In terms of the temperature field evolution, the temperature curves further reveal the impact of wall roughness on the combustion heat release process. Corresponding to the delayed pressure jumps, the abrupt temperature rise caused by the arrival of the flame front at each monitoring point is similarly and significantly delayed with increasing roughness. Overall, the flame temperature peaks influenced by rough walls are notably lower than those under the perfectly smooth wall (Ra = 0 mm) condition. Highly consistent with the pressure variations, during the early development stage at 90 mm, the temperature peak rises with increasing roughness; however, as the evolution proceeds to the mid-to-downstream sections (180 mm and 270 mm), the flame temperature induced by the 1 mm rough wall exhibits a downward trend, gradually falling below the 0.5 mm and 0.1 mm roughness cases.

Furthermore, it is clearly observable from the temperature curves that the time span of the high-temperature reaction zone is significantly prolonged as wall roughness increases. This phenomenon corroborates the fluid dynamic mechanism discussed previously: the strong shear vortices induced by the roughness elements greatly promote the development of the boundary layer flame, concentrating the flame, which would otherwise propagate toward the pipe center, in the near-wall region.


OH×10⁻³
×10³T(K)
H2 O2
6μs
5μs
4μs
3μs
2μs
1μs
Ignition
T
OH
H2
O2
Ra=0mm
Ra=0.1mm
Position(mm)
T(K)
H2
O2


OH×10⁻³×10³T(K)
H2 O2
6μs
5μs
4μs
Ignition
3μs
2μs
Position(mm)
Ra=0.5mm

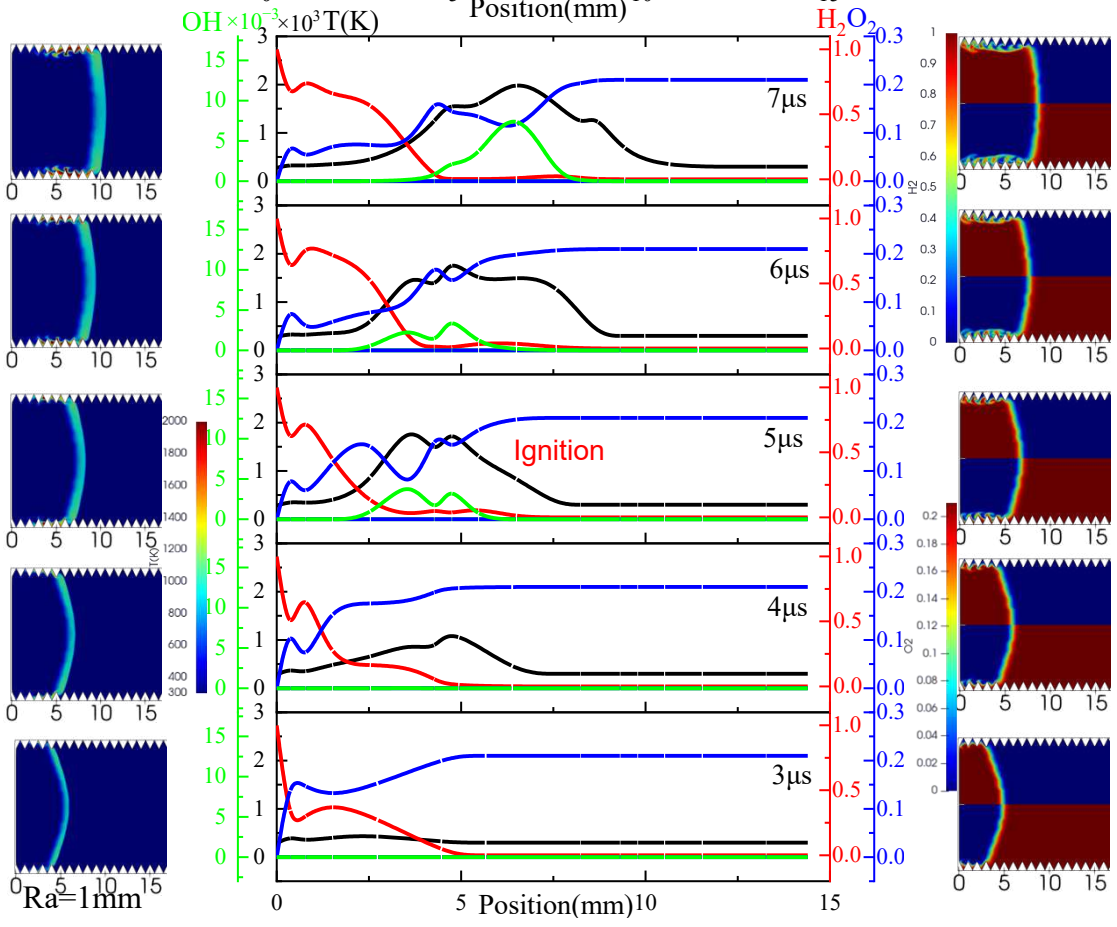

OH×10⁻³×10³T(K)
H2 O2
7μs
6μs
5μs
Ignition
4μs
3μs
Position(mm)
Ra=1mm

Fig. 6 Evolution of temperature and OH, H_2, and O_2 concentrations before and after ignition at 5.89 MPa burst pressure

Figure 6 illustrates the spatial and temporal transient evolution of temperature, OH radical concentration, and reactant (H_2 and O_2) concentrations during the initial ignition phase for four different wall roughness cases (Ra = 0, 0.1, 0.5, and 1 mm) under a 5.89 MPa burst pressure.

Under different wall roughness conditions, the ignition delay times and spatial ignition locations of the mixture are fundamentally similar, with only minor discrepancies; ignition occurs around 4 μs across all four cases. However, the exact spatial locations of ignition differ. For the perfectly smooth wall (Ra = 0) case, the temperature jump and OH radical generation (marked as Ignition) are observed at a spatial location of approximately 6 mm. With the introduction of wall roughness, the ignition location for the Ra = 0.1 mm case shifts to approximately 2.5 mm. As roughness further increases, the ignition locations for the Ra = 0.5 mm and Ra = 1 mm cases subsequently migrate downstream (to approximately 3–4 mm).

In the perfectly smooth (Ra = 0) case, once ignition is triggered, the OH radical concentration curve exhibits a steep, single-peak jump (peaking near 15×10^{-3} at 6 μs). This indicates an explosive generation of active radicals that dominates the high-frequency chain-branching reactions, resulting in a highly concentrated combustion zone. However, with increasing roughness, the structure of the reaction zone undergoes drastic changes. In the rough wall cases (Ra = 0.1, 0.5, and 1 mm), the generation of OH radicals no longer forms a single, concentrated sharp peak; instead, it evolves into a broader distribution over time, even manifesting a distinct “bimodal” (dual-peak) structure (e.g., Ra = 0.5 mm at 6 μs, and Ra = 1 mm at 7 μs). Concurrently, the peak concentration decreases substantially. For instance, the peak OH mole fraction for the Ra = 1 mm case at 2 μs post-ignition (i.e., at 7 μs) is only about 3×10^{-3}, far below the level observed at the same developmental stage for the smooth wall.

Observing the H_2 and O_2 concentration curves yields similar findings. At roughnesses of Ra = 0.5 mm and 1 mm, the flow field structure undergoes severe evolution. In the mid-to-late stages of evolution (e.g., 6 μs for Ra = 0.5, and 6 μs/7 μs for Ra = 1), the H_2 and O_2 concentration curves are not only spatially stretched (spanning over 5 mm) but their consumption processes also lose their monotonic smoothness. In the regions between the dual (or multiple) temperature peaks, the O_2 and H_2 concentrations exhibit significant local fluctuations and stagnation (e.g., localized rebounds in O_2 concentration). Correlating this with the 2D contours for the Ra = 0.5 mm and 1 mm cases, it is evident that the roughness elements induce intense microscopic vortices within their cavities. These vortices tear apart the previously continuous flame front. Large amounts of high-temperature products and

OH radicals are anchored and "trapped" within the near-wall roughness grooves, while the unburned cold mixture (H_2 and O_2) in the central region is entrained and drawn into the combustion product zone driven by shear layer instabilities (Kelvin-Helmholtz instability). This severe vortex entrainment highly wrinkles, folds, and even fractures the flame surface.

Simultaneously, the spatial distribution of the temperature curves for the rough wall cases becomes significantly broader. Specifically, the locations corresponding to the dual peaks in temperature and OH concentration reveal that the interaction between the shock wave and roughness elements leads to the formation of multiple local hotspots and reaction zones, spatially dispersing the originally concentrated heat release.

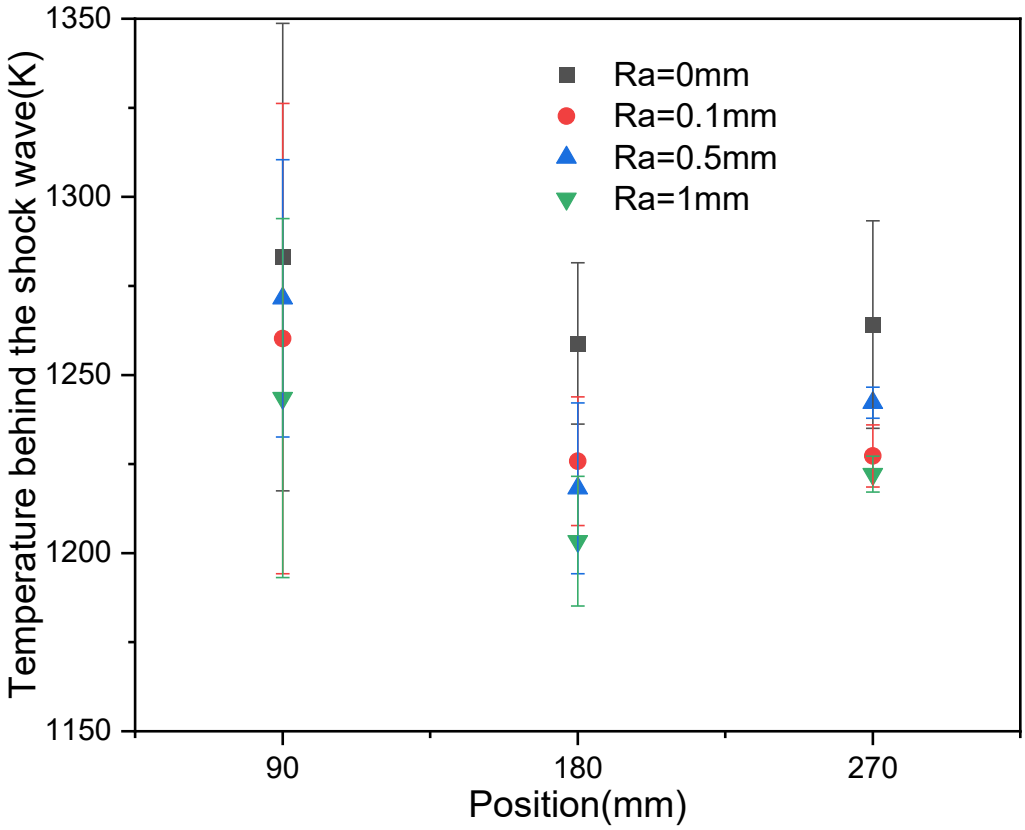


Fig.7 Post-shock temperatures for various wall roughnesses

Figure 7 compiles the distribution of the post-shock preheat zone temperature at three monitoring points (90 mm, 180 mm, and 270 mm) under a 5.89 MPa burst pressure for different wall roughnesses (Ra = 0, 0.1, 0.5, and 1 mm). It is evident that across all spatial locations, the overall post-shock temperature exhibits a decreasing trend with increasing wall roughness. For the perfectly smooth wall (Ra = 0 mm) case, the compression heating effect induced by the leading shock is the most intense, maintaining the highest post-shock temperatures at all monitoring points (e.g., reaching a maximum of approximately 1285 K at 90 mm). However, as

wall roughness is introduced and increased, this shock-induced heating potential is significantly attenuated. When Ra reaches 1 mm, the preheat zone temperature drops to the lowest level among all cases, plummeting below 1200 K at the 180 mm location.

The overall decline in post-shock preheat zone temperature with increasing roughness primarily stems from dual dissipation mechanisms in flow dynamics and thermodynamics. First, the wall roughness elements significantly increase the morphological drag of the near-wall flow, which not only attenuates the propagation kinetic energy of the leading shock wave but also induces intense microscopic vortex dissipation within the boundary layer. This direct attenuation of shock strength lowers the upper temperature limit to which the mixture can be shock-heated. Second, the increased roughness substantially expands the effective gas-solid contact area and drastically intensifies the turbulent convective heat transfer in the near-wall region, causing the high-temperature heat initially accumulated behind the shock to dissipate much more rapidly into the cold wall.

3.3 Effect of Wall Roughness on Ignition

Figure 8 records the evolutionary distribution of the post-shock preheat zone temperature as a function of burst pressure under different wall roughnesses (Ra = 0 to 1 mm). In the figure, dashed lines with hollow markers represent cases where the mixture failed to ignite at the corresponding burst pressure, while solid lines with solid markers trace the development of the post-shock preheat zone temperature following successful ignition. Overall, at a given burst pressure, the temperature of the post-shock preheat zone exhibits a distinct downward trend as wall roughness increases, consistent with the findings at 5.89 MPa discussed in Section 3.2. Near a burst pressure of 3.6 MPa, the post-shock temperature for the smooth wall (Ra = 0 mm) approaches 1080 K; whereas at a similar burst pressure of 3.5 MPa, the preheat zone temperature for the maximum roughness case (Ra = 1 mm) is only heated to approximately 985 K.

The rightward shift of the solid line starting points visually reflects the impact of roughness on the critical burst pressure required to successfully induce ignition. The critical burst pressure was identified as the minimum pressure capable of triggering ignition; in other words, a further pressure reduction of 0.1 MPa would result in an ignition failure. The smooth pipe (Ra = 0 mm) system can cross the ignition critical point at approximately 3.2 MPa. However, once wall roughness is present (whether Ra = 0.1 mm, 0.5 mm, or 1 mm), the critical burst pressure to successfully trigger ignition is elevated to 3.5 MPa. This jump in the ignition threshold is primarily attributed to the rough wall attenuating the leading shock strength and interfering with the initial flame kernel development within the boundary layer. Under the dual effects of severe energy dissipation and wall heat loss, the system must rely on a higher initial burst pressure to compensate for the

energy deficit required for ignition.

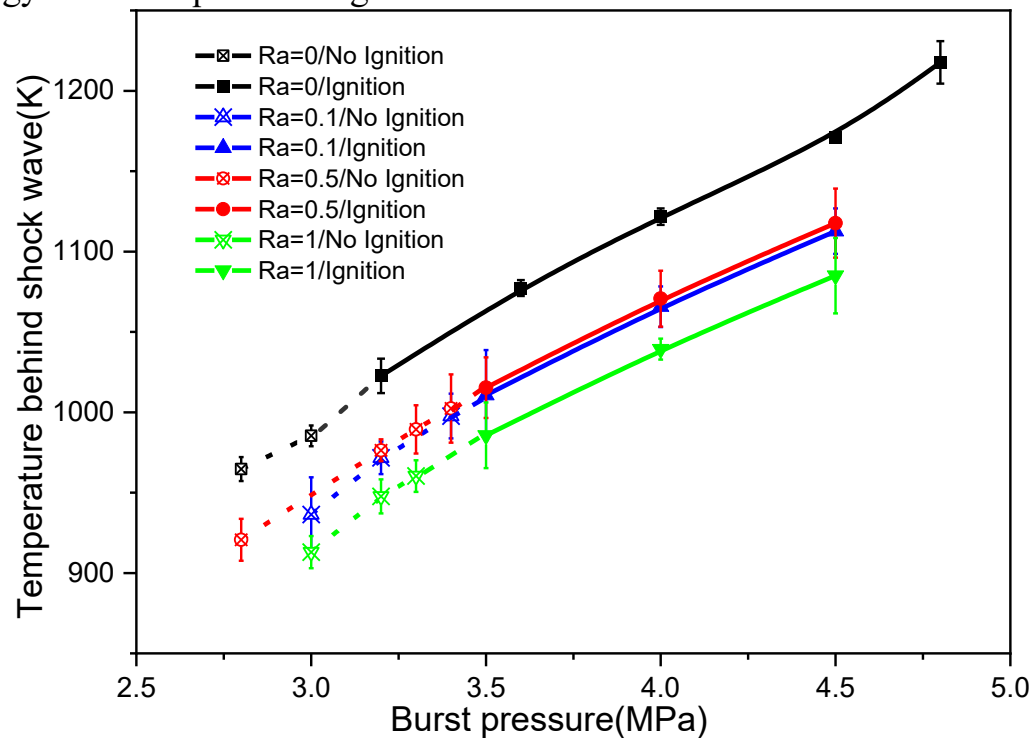


Fig. 8 Temperature behind shock wave as a function of burst pressure for various wall roughnesses

4. Conclusion

This paper focuses on the wall roughness factor in pressurized hydrogen tube systems. By incorporating a mixture averaged transport model and an improved Partially Stirred Reactor combustion model, the influence mechanisms of different wall roughnesses (Ra = 0, 0.1, 0.5, and 1 mm) on the entire process of pressurized hydrogen spontaneous ignition and subsequent flame dynamics were evaluated. The specific conclusions are as follows:

(1)Wall roughness significantly suppresses the tendency of the flame front to merge and expand toward the pipe center; the greater the roughness, the more pronounced the suppression. The central flame in the 1 mm case even exhibits distinct dissipation during the late stages of evolution. Conversely, roughness-induced instabilities generate massive vortices near the wall, intensifying the boundary layer combustion state and globally reducing the forward shock propagation speed in a non-linear manner (the 1 mm case exhibits the most severe suppression, while the 0.1 mm case suppresses the shock more than the 0.5 mm case).

(2)Rough walls cause a systematic delay in the arrival times of the shock wave and flame front at various spatial monitoring points. At the upstream section of the pipe (90 mm), peak pressure and temperature increase with roughness. However, as

the flow field propagates mid-to-downstream, excessive heat release and intense vortex dissipation in the boundary region consume system energy, causing the mean pressure and temperature in the high-roughness (1 mm) case to attenuate significantly, eventually reversing to drop below those of the lower-roughness cases.

(3)During the initial ignition phase, a smooth wall promotes an explosive, single-peak jump in OH radicals. In contrast, vortices in rough wall tear the originally continuous flame front, broadening the OH concentration distribution and lowering the peak concentration. This vortex entrainment disrupts the monotonic and smooth consumption of H_2 and O_2, spatially stretching the reaction zone and dispersing the originally concentrated heat release.

(4)Wall roughness elements not only attenuate the propagation kinetic energy of the leading shock wave but also intensify turbulent convective heat transfer in the near-wall region, leading to a drop in the post-shock preheat zone temperature as roughness increases. Subjected to the dual actions of energy dissipation and wall heat loss, rough walls necessitate a jump in the critical burst pressure threshold required for ignition, elevating it from approximately 3.2 MPa for a smooth pipe to 3.5 MPa.

Declaration of competing interest

The authors declare that they have no known competing financial interests or personal relationships that could have appeared to influence the work reported in this paper.

Acknowledgments

This research was supported by Key R&D Program of Zhejiang(2024C03252), Emergency Management R&D Program of Zhejiang(2025YJ005), and Science and Technology Program of Wenzhou(G20240078).

Reference

Bivol, G. Yu., Golovastov, S.V., Golub, V.V., 2024. Flame acceleration in rough narrow channels. Process Safety and Environmental Protection 191, 736–749. https://doi.org/10.1016/j.psep.2024.09.001

Bivol, G.Yu., Golovastov, S.V., Golub, V.V., 2024. Experimental investigation of detonation decay in rough narrow channels. International Journal of Hydrogen Energy 50, 1420–1429. https://doi.org/10.1016/j.ijhydene.2023.11.097

Burke, M.P., Chaos, M., Ju, Y., Dryer, F.L., Klippenstein, S.J., 2012. Comprehensive H_2 /O_2 kinetic model for high-pressure combustion. Int J of Chemical Kinetics 44, 444–474. https://doi.org/10.1002/kin.20603

Huang, S., Li, Q.S., 2010. A new dynamic one-equation subgrid-scale model

for large eddy simulations. Numerical Meth Engineering 81, 835–865. https://doi.org/10.1002/nme.2715

Ingenito, A., Bruno, C., 2010. Physics and Regimes of Supersonic Combustion. AIAA Journal 48, 515–525. https://doi.org/10.2514/1.43652

Kajishima, T., Nomachi, T., 2006. One-Equation Subgrid Scale Model Using Dynamic Procedure for the Energy Production. Journal of Applied Mechanics 73, 368–373. https://doi.org/10.1115/1.2164509

Kim, S.-E., n.d. Large Eddy Simulation Using an Unstrcutured Mesh Based Finite-Volume Solver.

Li, Q., Hu, H., Pan, Z., Ciccarelli, G., 2026. Transition from a fast-flame to detonation in a rough-walled channel. Combustion and Flame 283, 114604. https://doi.org/10.1016/j.combustflame.2025.114604

Liu, N.-S., Lu, X.-Y., 2005. Large eddy simulation of turbulent flows in a rotating concentric annular channel. International Journal of Heat and Fluid Flow 26, 378–392. https://doi.org/10.1016/j.ijheatfluidflow.2004.10.005

Luo, G., Zhang, W., Yang, Z., Zhang, L., Zhang, J., 2025. Transport models for predicting spontaneous ignition of pressurized hydrogen released into a tube. Case Studies in Thermal Engineering 73, 106548. https://doi.org/10.1016/j.csite.2025.106548

Maeda, S., Fujisawa, M., Ienaga, S., Hirahara, K., Obara, T., 2019. Effect of sandpaper-like small wall roughness on deflagration-to-detonation transition in a hydrogen–oxygen mixture. Proceedings of the Combustion Institute 37, 3609–3616. https://doi.org/10.1016/j.proci.2018.07.119

Qi, H., Li, X., Hu, R., Yu, C., 2022. Quasi-dynamic subgrid-scale kinetic energy equation model for large-eddy simulation of compressible flows. Journal of Fluid Mechanics 947, A22. https://doi.org/10.1017/jfm.2022.654

Ranjan, R., Venkataswamy, M.K., Menon, S., 2020. Dynamic one-equation-based subgrid model for large-eddy simulation of stratified turbulent flows. Phys. Rev. Fluids 5, 064601. https://doi.org/10.1103/PhysRevFluids.5.064601

Rudy, W., Dabkowski, A., Teodorczyk, A., 2014. Experimental and numerical study on spontaneous ignition of hydrogen and hydrogen-methane jets in air. International Journal of Hydrogen Energy 39, 20388–20395. https://doi.org/10.1016/j.ijhydene.2014.05.077

Wang, M., Li, Q., Wen, X., Guo, Z., Zhong, F., Ding, X., 2026. Flame propagation and explosion characteristics of NH3/H2/air mixtures in pipes: Effects of wall roughness on late-stage tulip-flame evolution. Process Safety and Environmental Protection 210, 108695. https://doi.org/10.1016/j.psep.2026.108695

Xiang, Z., Yang, S., Xie, S., Li, J., Ren, H., 2020. Turbulence–chemistry interaction models with finite-rate chemistry and compressibility correction for simulation of supersonic turbulent combustion. Engineering Applications of

Computational Fluid Mechanics 14, 1546–1561. https://doi.org/10.1080/19942060.2020.1842248

Yan, C., Ng, H.D., Mi, X., 2023. A numerical study on the influence of increased instability of quasi-detonation on the critical tube diameter phenomenon. Proceedings of the Combustion Institute 39, 2835–2845. https://doi.org/10.1016/j.proci.2022.11.007

Zhang, Y., Zheng, X., Xiang, G., 2026. Active control of oblique detonation waves through engineered wall properties. Aerospace Science and Technology 171, 111684. https://doi.org/10.1016/j.ast.2026.111684

Zhao, M., Liu, D., Li, M., Xiao, H., 2024. Effect of wall roughness on flame acceleration and deflagration-to-detonation transition in a narrow channel. International Journal of Hydrogen Energy 51, 880–893. https://doi.org/10.1016/j.ijhydene.2023.05.198

Zhong, C., Gou, X., 2021. Inhibition Mechanism of CH_4 Addition on the Pressurized Hydrogen Spontaneous Ignition. Energy Fuels 35, 1715–1726. https://doi.org/10.1021/acs.energyfuels.0c03282